Crystallization-Induced Undulated Morphology in Polystyrene-*b*-Poly(L-lactide) Block Copolymer

Rong-Ming Ho,*,†,‡ Fang-Ho Lin,† Chi-Chun Tsai,§ Chu-Chieh Lin,|| Bao-Tsan Ko,‡ Benjamin S. Hsiao,⊥ and Igors Sics⊥

Department of Chemical Engineering, National Tsing-Hua University, Hsinchu 30013, Taiwan, Union Chemical Laboratories, Industrial Technology Research Institute, Hsinchu 30013, Taiwan, Department of Chemical Engineering, National Chung-Hsing University, Taichung 402, Taiwan, Department of Chemistry, National Chung-Hsing University, Taichung 402, Taiwan, and Department of Chemistry, State University of New York at Stony Brook, Stony Brook, New York 11794-3400

Received April 13, 2004; Revised Manuscript Received June 3, 2004

ABSTRACT: The crystallization of the PLLA block within the microphase-separated lamellar microdomain in a poly(styrene)-*b*-poly(L-lactide) (PS-PLLA) diblock copolymer was carried out from hard confinement (i.e., the crystallization temperature of PLLA ($T_{c,PLLA}$) < the glass transition temperature of PS ($T_{g,PS}$)) to soft confinement (i.e., $T_{c,PLLA} \geq T_{g,PS}$), where interesting morphological evolution was observed. At $T_{c,PLLA} < T_{g,PS}$, a typical confined morphology was obtained, while at $T_{c,PLLA} \geq T_{g,PS}$, a unique undulated morphology was seen for the first time. The amplitude and periodicity of the undulation instability are dependent upon the orientation of microphase-separated lamellae. The PLLA crystals under confinement formed perpendicular morphology having crystalline chains normal to the lamellae as evidenced by 2D small-angle X-ray scattering and wide-angle X-ray scattering. On the basis of morphological observations and crystallization kinetics studies, the undulation instability can be attributed to the change of crystallization mechanism from hard to soft confinement, which coincides with the transition from homogeneous to heterogeneous nucleation.

Introduction

The self-assembly behavior of block copolymers has been extensively studied due to their abilities to self-organize into one-, two-, and three-dimensional periodic nanostructures in bulk with different compositions (i.e., volume fraction).[1] The distinct nanostructures that can be tailored by molecular engineering in synthetic block copolymers are particularly appealing for the applications of nanotechnology.[2] In the block copolymer studies, the crystallization process of one or more blocks provides an additional pathway to modify the microphase-separated morphology, which can lead to the modulation of properties in nanostructured microdomains through crystallinity. Because the competition between crystallization and microphase separation is critical to determine the final morphology of crystallizable block copolymers, extensive studies have also been carried out to understand the intricate effects of confinement on crystallization, as well as of crystallization on the final nanostructures.[3−30] It was evident that the final morphology was found to be strongly dependent upon the experimental temperature, with respect to the order−disorder transition temperature (T_{ODT}), the crystallization temperature of the crystallizing block (T_c^c), the glass transition of the amorphous block (T_g^a), and the crystallization rate. In other words, the final morphology is the consequence of microphase separation, crystallization, and vitrification.

To be specific, when $T_c^c > T_{ODT} > T_g^a$, it is generally agreed that the final morphology is driven by crystallization regardless of microphase separation.[3−6] For systems with $T_{ODT} > T_g^a > T_c^c$ (this is a hard confinement for crystallization),[7−19] the ordered nanostructure can be preserved due to the vitrified microdomains of amorphous blocks. In contrast, if $T_{ODT} > T_c^c \geq T_g^a$, the effect of crystallization on the morphological changes becomes more complicated (this is a soft confinement).[20−30] In this case, the segregation strength of microphase separation usually determines the crystalline morphology. In addition, the final morphology is a strong function of the confined features and the morphology of nanostructures.[30] In extremely strong segregation (i.e., ratio of $(\chi N)_{T_c}$ and $(\chi N)_{T_{ODT}} \gg 3$, where χN is the product of incompatibility between the constituted block and the molecular weight of block copolymer)[30] of various phase-separated morphology, it is commonly agreed that ordered nanostructure can be maintained regardless of crystallization. In intermediate to strong segregation strength (ratio of $(\chi N)_{T_c}$ and $(\chi N)_{T_{ODT}} > 3$), there are still some disagreements as to what will dominate the crystallized morphology. For example, the microphase-separated nanostructure can be preserved or templated or even broken out by crystallization. In the present study, an interesting new undulated morphology induced by crystallization in lamellar structures was observed in a PS-PLLA block copolymer, where strong segregation strength exists and the glass transition temperature of PS ($T_{g,PS}$) is located within the crystallization window (the schematic diagram of the two pathways leading to different morphology is shown in Figure 1). A confined morphology for crystallized PS-PLLA was observed when the crystallization temperature of PLLA ($T_{c,PLLA}$) was less than $T_{g,PS}$. However, the microphase-separated lamellar microdomains became undulated by crystallization once $T_{c,PLLA}$ was near or

* To whom correspondence should be addressed. Phone: 886-3-5738349. Fax: 886-3-5715408. E-mail: rmho@mx.nthu.edu.tw.
† National Tsing-Hua University.
‡ Union Chemical Laboratories.
§ Department of Chemical Engineering, National Chung-Hsing University.
|| Department of Chemistry, National Chung-Hsing University.
⊥ State University of New York at Stony Brook.

10.1021/ma0492869 CCC: $27.50
Published on Web 07/17/2004

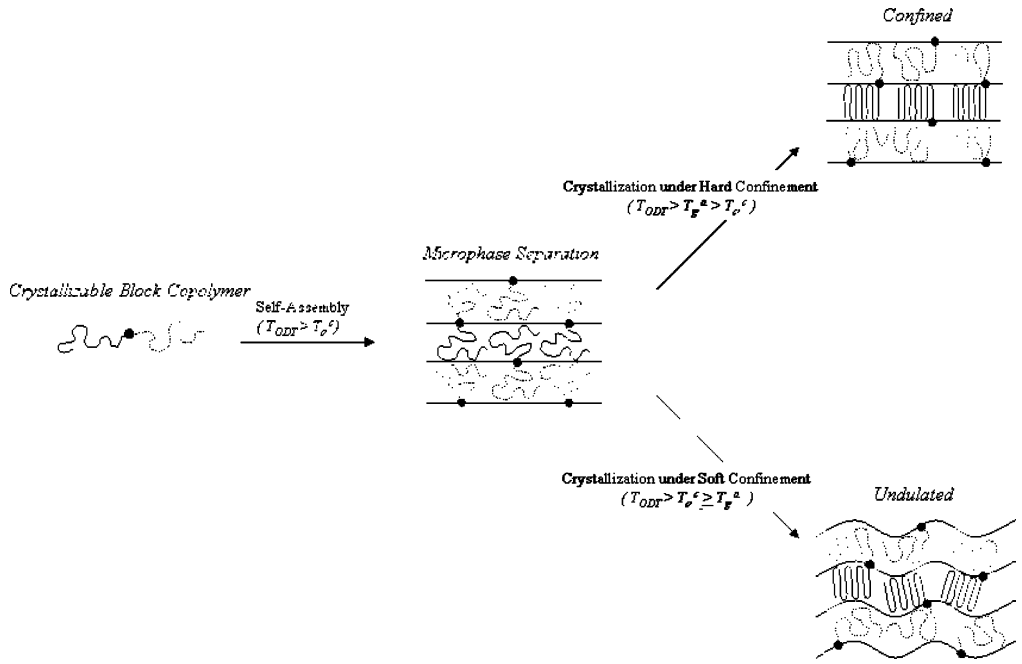

Figure 1. Competition between the driving force of crystallization and the segregation strength of microphase separation.

above $T_{g,PS}$. The crystallization-induced undulation of the lamellar morphology gave rise to significant changes in crystallization and melting behavior. The origin of the lamellar undulation can be attributed to the change of crystallization mechanism from hard to soft confinement, which coincides with the transition from homogeneous to heterogeneous nucleation.

Experimental Section

Materials. Crystallizable diblock copolymers, PS-PLLA, have been synthesized by sequential living free radical polymerization and ring-opening polymerization.[32] Free radical polymerization of styrene using 4-hydroxy-2,2,6,6-tetramethylpiperidine-*N*-oxyl, 4-hydroxy-TEMPO (4-OH-TEMPO), as an initiator in the presence of dibenzoylperoxide (BPO) resulted in a hydroxyl-terminated polystyrene. The PS-TEMPO-4-OH was further reacted with $[(\mu_3\text{-EDBP})Li_2]_2[(\mu_3\text{-}^n\text{Bu})Li(0.5Et_2O)]_2$ giving a macroinitiator. The $[(\mu_3\text{-EDBP})Li_2]_2$ $[(\mu_3\text{-}^n\text{Bu})Li(0.5Et_2O)]_2$ was prepared according to the method described previously.[31] Followed by the controlled ring-opening polymerization of L-lactide in the presence of the macroinitiator, PS-PLLA was then prepared. The detailed synthetic routes and conditions were reported in our recent paper.[32]

The gel permeation chromatography (GPC) measurements were performed on a Hitachi L-7100 system equipped with a differential Bischoff 8120 RI detector using THF (HPLC grade) as an eluent. Molecular weight and molecular weight distributions were calculated using polystyrenes as standards. The number average molecular weight of 4-hydrolysis-TEMPO terminated PS and the polydispersity (PDI) of PS-PLLA block copolymer were determined as 13 300 g/mol and 1.13, respectively, by the GPC analysis. The molecular weight of PLLA blocks was determined as 21 700 g/mol by the ^{1}H NMR analysis. The volume fraction of PLLA calculated, by assuming the densities of PS and PLLA are 1.02 and 1.18 g/cm^3, was 0.585 in the molten state. For comparison purposes, PLLA homopolymer was also synthesized using living ring-opening polymerization as described above. The molecular weight of PLLA homopolymer and PDI was determined to be 21 200 g/mol by ^{1}H NMR analysis and 1.05 by GPC.

Sample Preparation. Bulk samples of block copolymers were prepared by the casting method using dichloromethane (CH_2Cl_2) solution (10 wt % of PS-PLLA) at room temperature in a beaker and were thermally treated in the vacuum oven for 12 h to remove the residual solvent. Crystallization of PLLA in PS-PLLA gave rise to a significant change for microphase-separated morphology of PS-PLLA as observed. To eliminate the possible effect of PLLA crystallization on formed morphology, cast samples were annealed at a temperature (160 °C for 3 min) above the PLLA melting but below the order−disorder transition temperature, and then rapidly cooled at a rate of 150 °C/min to room temperature. No significant degradation was found as measured by the GPC analysis. The order−disorder transition temperature of PS-PLLA was above the degradation temperature (∼170 °C) as identified by small-angle X-ray scattering (SAXS). Time-resolved SAXS experiments were carried out in a heating chamber with the step-temperature increasing. The degradation temperature was identified by the disappearance of the scattering peaks.

The orientation of single-domain-like block copolymer nanostructures was achieved by a novel rimming coating method as follows. 10 wt % PS-PLLA in dichloromethane solution was first placed in an open test tube fixed on a spin coater, and then spin-coated at 1200 rpm to achieve the molecular orientation. The schematic diagrams of using the rimming coating method to orient PS-PLLA samples are illustrated in Figure 2. After coating, the samples were thermally treated as described above.

Transmission Electron Microscopy (TEM). Thin sections of solution-cast or rimming-coated PS-PLLA bulk samples having a thickness of about 70 nm were obtained by ultracryomicrotomy using a Reichert Ultracut microtome. Bright field transmission electron microscopy (TEM) images were obtained using the mass-thickness contrast with a JEOL TEM-1200x transmission electron microscope (at an accelerating voltage of 120 kV). Staining was accomplished by exposing the samples to the vapor of a 4% aqueous RuO_4 solution for 2 h.

Synchrotron X-ray Experiments. Simultaneous 2D wide-angle X-ray scattering (WAXS) and SAXS experiments were conducted at the synchrotron X-ray beamline X27C at the National Synchrotron Light Source (NSLS) in Brookhaven National Laboratory (BNL). The wavelength of the X-ray beam was 0.1366 nm. A MAR CCD X-ray detector (MAR) was used to collect the 2D SAXS patterns. A 1D linear profile was obtained by integration of the 2D pattern. The scattering angle of the SAXS pattern was calibrated using silver behenate, with the first-order scattering vector q^* ($q^* = 4\pi\lambda^{-1} \sin\theta$, where 2θ is the scattering angle) being 1.076 nm^{-1}. The diffraction peak positions and the widths observed from WAXS experiments were carefully calibrated with silicon powder with 2θ being 28.4° under Cu Kα radiation. Azimuthal profiles were extracted from 2D WAXS patterns for further analysis.

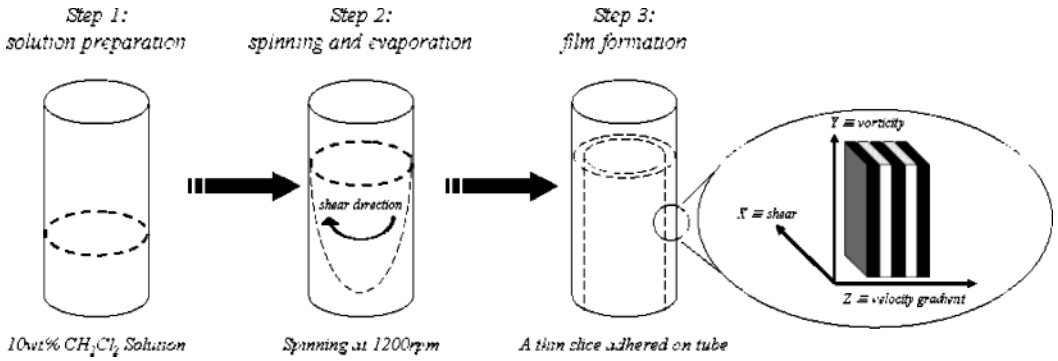

Figure 2. Illustration of rimming flow and the orientation of lamellar microstructure.

Differential Scanning Calorimetry (DSC). DSC experiments were carried out in a Perkin-Elmer DSC 7 equipped with an intracooler and calibrated with cyclohexane and indium for the measurements of thermal behavior of PS-PLLA. The melting point of the PLLA blocks in PS-PLLA was around 150 °C. The glass transition temperatures of PLLA and PS were approximately 45 and 85 °C, respectively. All of the measurements were carried out at the heating rate of 10 °C/min. The relative crystallinity of PLLA (w^c) was determined by the equation $w^c = \Delta H_m(t)/(w_E \Delta H_{m,f})$, where w_E is the weight fraction of the PLLA block, and ΔH_m is the heat of melting of 100 wt % crystalline PLLA (93 J/g).[33]

Results and Discussion

Lamellar Morphology of PS-PLLA. Bulk samples of block copolymers were first prepared by solution casting. Upon being quenched from the microphase-separated states, the thermally annealed samples (at 160 °C) were studied by scattering measurements. Also, the samples sectioned by ultra-microtome at room temperature were examined by TEM microscopy. Both TEM (Figure 3a) and SAXS (Figure 3b) clearly showed the lamellar structure. In the TEM image, the microdomains of the PS phase appear dark due to the staining of RuO_4, while the microdomains of PLLA appear light. The corresponding SAXS pattern confirms the lamellar structure because the scattering peaks occur at q^* ratios of 1:2:3:4.

Undulation in Morphology Induced by Crystallization. To examine the effect of PLLA crystallization on the microphase-separated morphology, the samples were first melted and then quenched to a temperature range between the melting temperature (~150 °C) and the glass transition temperature of PLLA (~45 °C) using the following procedures. The samples were first annealed at 160 °C to eliminate thermal history, and then rapidly cooled to a desired temperature for crystallization. The segregation strength of microphase separation was evaluated by the ratio of $(\chi N)_{T_c}$ to $(\chi N)_{T_{ODT}}$, where χ is the Flory segmental interaction parameter and N is the total degree of polymerization of the diblock polymer, using the procedures outlined before.[17] The interaction parameter of PS and PLA has been reported earlier, $\chi(T) = 98.1/T - 0.112$.[34] Assuming that the solubility parameters betweem PLA and PLLA are similar, then the value of $(\chi N)_{T_c}/(\chi N)_{T_{ODT}}$ within the crystallization window of PLLA (70−100 °C) should be around four or five. Thus, the crystallization within microphase-separated microdomains ($(\chi N)_{T_c}/(\chi N)_{T_{ODT}} > 3$) can be thought of as a process under strong segregation. In other words, the effect of phase incompatibility is expected to be very significant to influence the spatial confinement for the crystallization process of the PLLA blocks.

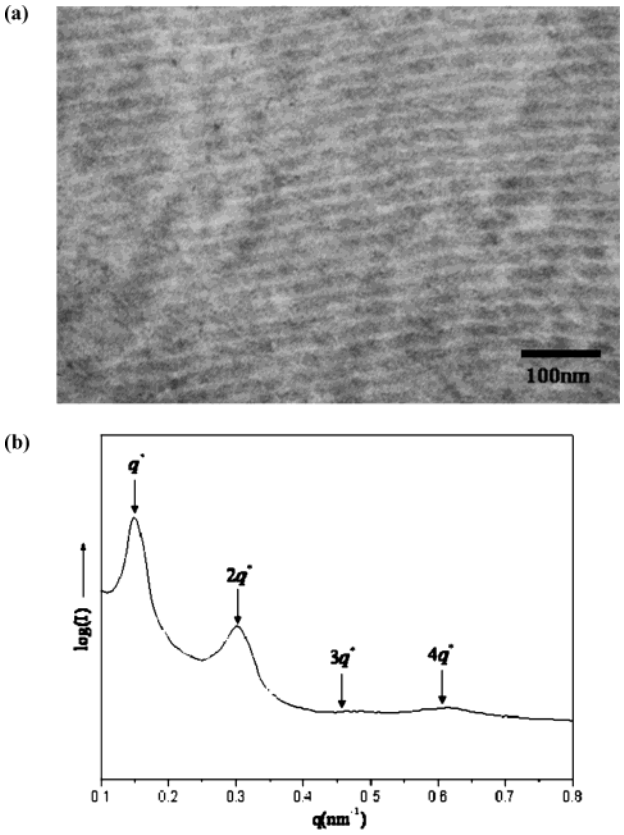

Figure 3. TEM micrograph (a) and SAXS pattern (b) of unoriented PS-PLLA samples quenched from ordered melt at 160 °C.

An interesting morphological evolution was observed in this study, depending on the experimental temperature with respect to $T_{c,PLLA}$ and $T_{g,PS}$. These observations are illustrated in Figure 4. When $T_{c,PLLA} < T_{g,PS}$ (i.e., hard confinement), the microphase-separated lamellar morphology is found to persist after crystallization, as indicated in Figure 4a. However, an undulation of lamellar morphology begins to form when $T_{c,PLLA}$ approaches $T_{g,PS}$ (Figure 4b). It appears that the reduced restraint in crystallizable PLLA blocks at the connected junctions of the incompatible microdomains probably increases the mobility of the entire block copolymer chain (from the glassy to the rubbery state), resulting in an undulation of lamellar morphology (Figure 4c) driven by the crystallization process at $T_{c,PLLA} > T_{g,PS}$ (i.e., soft confinement). This is quite reasonable because the crystalline morphology under confinement is strongly dependent upon the confined environment in addition to the phase behavior due to the incompatibility effect.

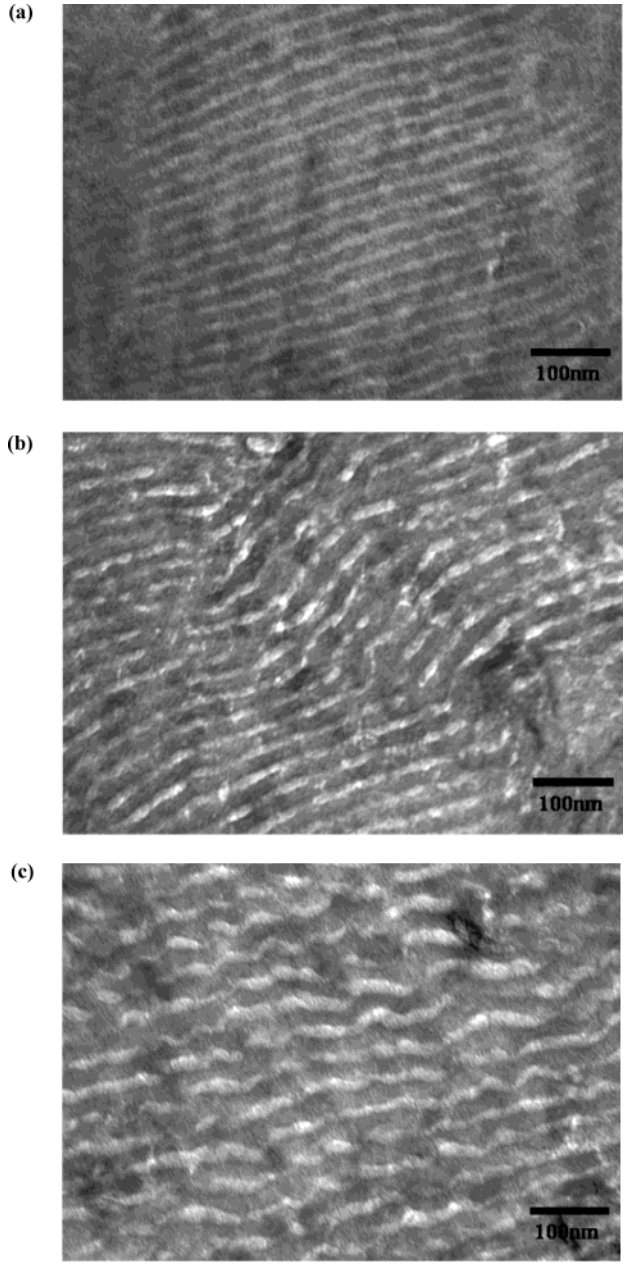

Figure 4. TEM micrographs of unoriented PS-PLLA samples (a) crystallized at 70 °C ($T_{c,PLLA} = 70$ °C < $T_{g,PS} \approx 85$ °C, under hard confinement); (b) crystallized at 85 °C ($T_{c,PLLA} \approx T_{g,PS}$, under soft confinement); and (c) crystallized at 100 °C ($T_{c,PLLA} > T_{g,PS}$, under soft confinement) from ordered melt at 160 °C.

Crystallization-induced undulation occurs once the crystallization temperature of PLLA surpasses the glass transition of the confined PS domains, which indicates that the ratio of $T_{c,PLLA}$ and $T_{g,PS}$ plays a critical role in determining the final morphology after the crystallization of PLLA. The change of the chain mobility in crystallization from hard to soft confinement inevitably affects crystallization behavior, which is discussed below.

Crystal Orientation in Nanostructure. To examine the relationship between crystallographic details of crystalline PLLA under confinement and the corresponding morphology, the oriented microdomains of the microphase-separated PS-PLLA sample were prepared as described in the Experimental Section. The oriented sample was studied by the combined SAXS and WAXS measurements. Figure 5a−c shows 2D SAXS patterns taken along the shear, vorticity, and gradient directions, designated as *x*, *y*, and *z*, respectively. The strong anisotropy in these patterns indicated that oriented microphase-separated microdomains were obtained after the coating process. For SAXS patterns along the *x* and *y* directions, both patterns are practically identical, showing a distinct lamellar morphology with a q^* ratio of 1:2:3:4 being observed. In contrast, only a weak SAXS diffraction peak in the 2D SAXS pattern along the *z* direction (i.e., parallel to the gradient direction) was observed. These results suggest that the macroscopically aligned sample, where the microphase-separated lamellar normal is parallel to the *z* direction (i.e., normal direction of tube surface) as shown in Figure 2, was obtained even if the orientation is not perfect. Corresponding WAXS results along the *x*, *y*, and *z* directions (Figure 5d−f) on the aligned sample were also obtained from isothermally crystallized samples annealed at temperatures below $T_{g,PS}$ (i.e., hard confinement) from the microphase-separated melt. Confined crystallization is identified as where crystallization occurs under spatial confinement by the glassy PS layers; microphase-separated lamellar morphology remains after crystallization. Similar to the SAXS results, the 2D WAXS patterns taken along the *x* and *y* directions are practically identical and exhibit distinct oriented features. However, only an isotropic ring along the *z* direction was observed. These results indicate that the PLLA crystals form specific orientation with respect to the *x* and *y* directions but exhibit random orientation along the *z* direction. On the basis of the α form of PLLA crystals having a unit cell of $a = 1.07$ nm, $b = 0.595$ nm, $c = 2.78$ nm, and $\alpha = \beta = \gamma = 90°$,[35,36] the observed reflections could be indexed as (003), (200), (110), and (203) with a pseudo-orthorhombic crystalline structure. The azimuthal profiles of these reflections were obtained from the 2D WAXS pattern (Figure 6a). It is seen that the maximum diffraction intensity of the (003) reflection locates at the azimuthal angle, $\Phi = 0°$ and 180°; that of the (200) and (110) reflections is at $\Phi = 90°$ and 270°; and that of the (203) reflection is at $\Phi = 60°$, 120°, 240°, and 300°. The schematic 2D WAXD pattern is illustrated in Figure 6b, which is consistent with a typical fiber diffraction pattern. This suggests that the PLLA crystalline chain alignment is uniaxial, having an orientation parallel to the microphase-separated lamellar normal (i.e., along the *z* direction). A schematic real-space model of the molecular disposition in the PLLA crystals is illustrated in Figure 7.

Similar results have been found for crystallized PS-PLLA samples annealed at different temperatures above $T_{g,PS}$ (i.e., soft confinement where the undulated lamellar morphology was seen), as illustrated in Figure 8 (sample crystallized at 100 °C). Unlike the morphological change seen in TEM, no significant discrepancy in crystal orientation has been observed for PLLA crystallization from hard to soft confinement (i.e., from low to high crystallization temperatures). However, in Figure 8, two extra (010) and (103) reflections were identified. The maximum intensity of the (103) reflection is located at $\Phi = 42°$, 141°, 220°, and 323°, and that of the (010) reflection is located at $\Phi = 94°$, 263°. It seems that the appearance of extra reflections can be mainly attributed to the perfection of the PLLA crystalline structure formed at higher temperatures. In other words, the crystalline PLLA chains adopt a perpendicular orientation with respect to the lamellar plane when

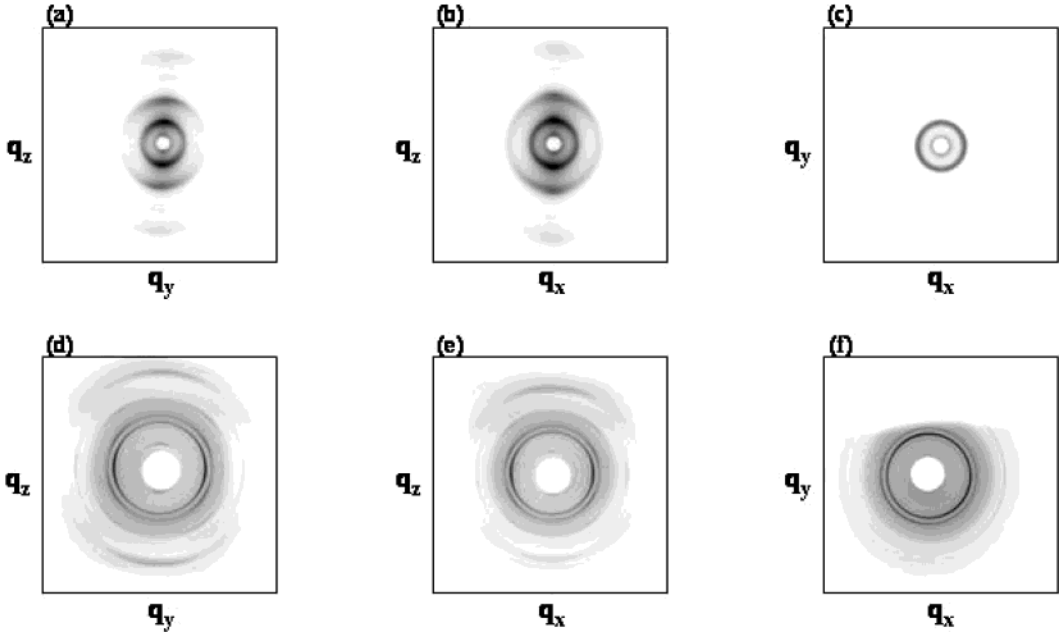

Figure 5. X-ray scattering patterns of oriented PS-PLLA samples isothermally crystallized at 70 °C from ordered melt at 160 °C. (a) 2D SAXS obtained when the X-ray beam is along the *X*-direction; (b) 2D SAXS along the *Y*-direction; (c) 2D SAXS along the *Z*-direction; (d) 2D WAXS along the *X*-direction; (e) 2D WAXS along the *Y*-direction; and (f) 2D WAXS along the *Z*-direction.

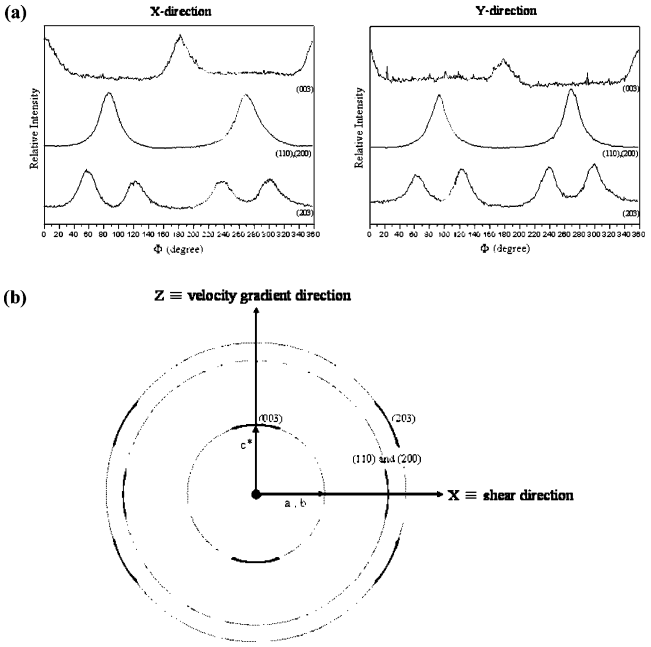

Figure 6. (a) Azimuthal profiles for the 2-D WAXS pattern of oriented PS-PLLA samples isothermally crystallized at 70 °C from ordered melt at 160 °C along the *X*-direction and *Y*-direction, respectively. Corresponding reflections are indicated as shown. (b) Schematic of the 2-D WAXS pattern.

formed under the confinement either of rigid PS layers (i.e., crystallized at low temperature) or of soft PS layers (i.e., crystallized at high temperature). The long periods of crystallized samples at different temperatures were determined, and the results are shown in Figure 9 where no significant change was seen.

Undulation in the Oriented Microdomains. For comparison purposes, oriented PS-PLLA samples were also examined by TEM to study the undulation phenomenon, as described for unoriented samples. Similar to unoriented samples, confined morphology was identified when $T_{c,PLLA} < T_{g,PS}$ (Figure 10a) where the undulated morphology was observed when $T_{c,PLLA} \geq T_{g,PS}$ in the oriented samples (Figure 10b). However, morphological undulation in oriented samples appears to have a much smaller amplitude when compared with the wavy layered morphology formed during crystallization of unoriented sample. These results indicate that the undulation induced by crystallization is affected by the grain size of the microdomains. It is conceivable that after rimming coating, the formation of large-scale oriented PS-PLLA microdomains alleviates the effect of crystallization-induced undulation, which can be explained as follows.

Crystallization Kinetics and Melting. The dynamic process of isothermal crystallization under confinement was monitored by the enthalpy change in DSC. As shown in Figure 11, the curve of exothermic response with crystallization time exhibits a noticeable transition from low to high crystallization temperature. At lower crystallization temperatures (temperature below 90 °C), the exothermic curve exhibits the exponential-like crystallization kinetics. In contrast, the exothermic curve gradually exhibits the sigmoidal crystallization kinetics for crystallization at higher temperatures (for instance, temperature above 90 °C). Crystallization halftimes, $t_{1/2}$, for PS-PLLA crystallized at different temperatures are plotted in Figure 12. When compared to PLLA homopolymer, the halftime significantly increases in the block copolymer, which is due to the retardation of crystallization in PLLA blocks under confinement.

To further examine the crystallization behavior, the temperature dependence of the Avrami exponent is determined. Crystallization kinetics was fitted by the typical Avrami equation.

$$1 - v_c = \exp(-kt^n) \qquad (1)$$

where v_c represents the volume fraction of the crystallization process that has occurred at time t, k is the rate constant, and n is the Avrami exponent. It is seen that the Avrami exponent increases with the crystallization temperature (Figure 13). At low crystallization temper-

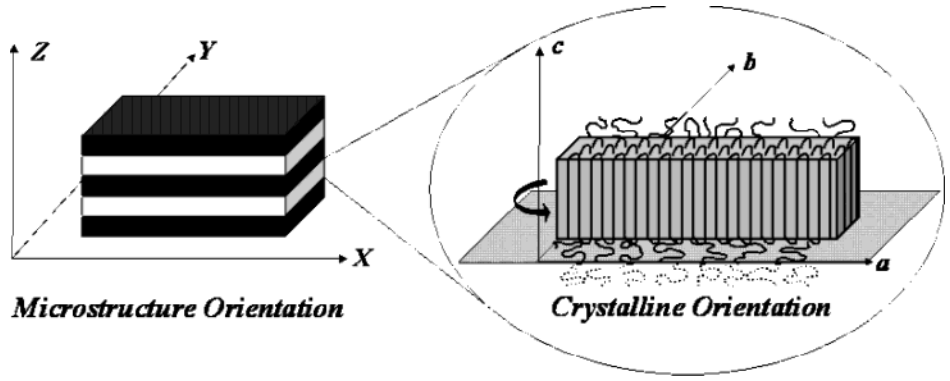

Figure 7. Molecular disposition of PLLA crystalline chain corresponding to the lamellar interface.

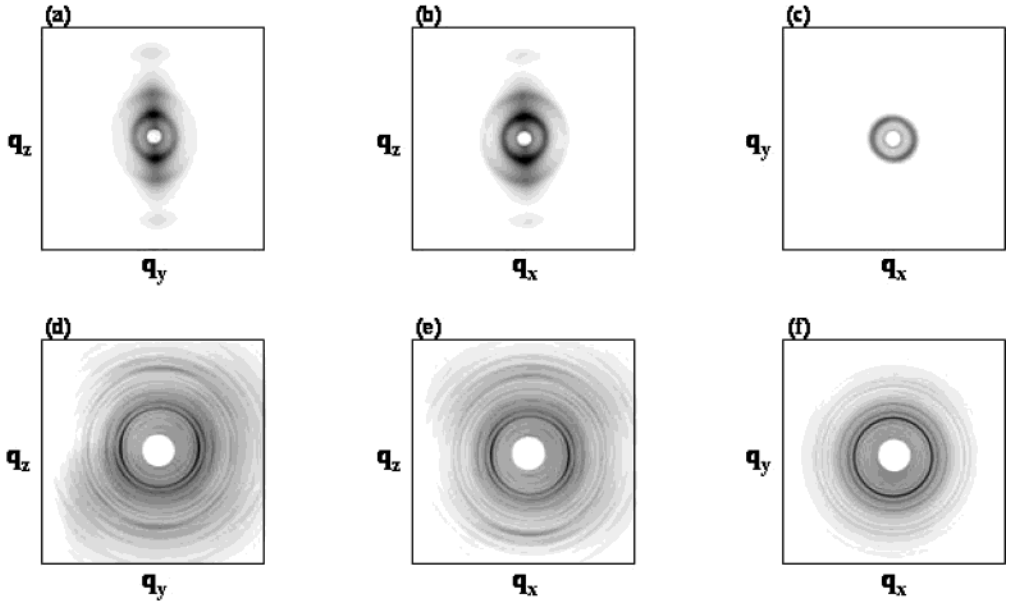

Figure 8. X-ray scattering patterns of oriented PS-PLLA samples isothermally crystallized at 100 °C from ordered melt at 160 °C. (a) 2D SAXS obtained when the X-ray beam is along the *X*-direction; (b) 2D SAXS along the *Y*-direction; (c) 2D SAXS along the *Z*-direction; (d) 2D WAXS along the *X*-direction; (e) 2D WAXS along the *Y*-direction; and (f) 2D WAXS along the *Z*-direction.

atures, the Avrami exponent is close to 1, which is a typical value for homogeneous nucleation of confined crystallization. Increasing the crystallization temperature gradually increases the value of the Avrami exponent. Similar to the transition of the rate of nucleation and of the crystallization rate, the change of Avrami exponent also exhibits a significant transition when $T_{c,PLLA}$ approaches or surpasses $T_{g,PS}$. The increase in crystallization temperature was found to raise the Avrami exponent to above 2. For homopolymer PLLA, the crystallization kinetics is dominated by the heterogeneous nucleation process, where the Avrami exponent is near a typical value of 3. In the case of PLLA-PS block copolymers, it is likely that the crystallization behavior is strongly affected by the confined environment, where the crystallization process would possess a slower crystallization rate and lower Avrami exponent. Thus, it is conceivable that the nucleation process gradually transforms from homogeneous to heterogeneous dominated nucleation processes in the chosen PS−PLLA block copolymer with the increase in the crystallization temperature.

Figure 14 shows the plot of the melting temperature as a function of the crystallization temperature. The melting point of crystallized PLLA under confinement in block copolymer is significantly lower than that of homopolymer PLLA. This is expected for the following reasons. For homopolymer PLLA, the melting temperature increases linearly with the crystallization tem-

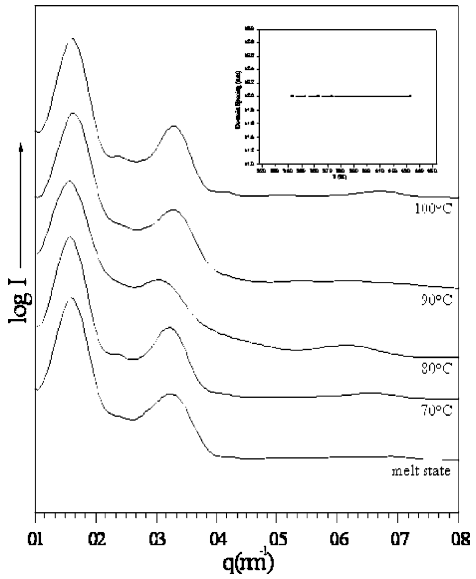

Figure 9. One-dimensional SAXS profiles of PS-PLLA samples isothermally crystallized at different temperatures and quenched sample from ordered melt at 160 °C. The inset shows the change of long period with crystallization temperature.

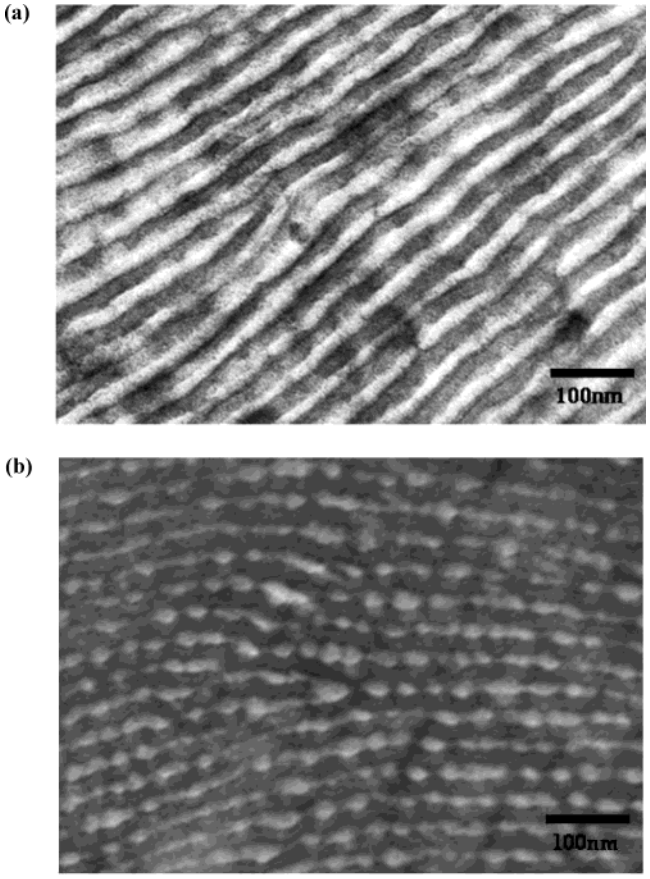

Figure 10. TEM micrographs of oriented PS-PLLA samples (a) crystallized at 70 °C; and (b) crystallized at 100 °C from ordered melt at 160 °C.

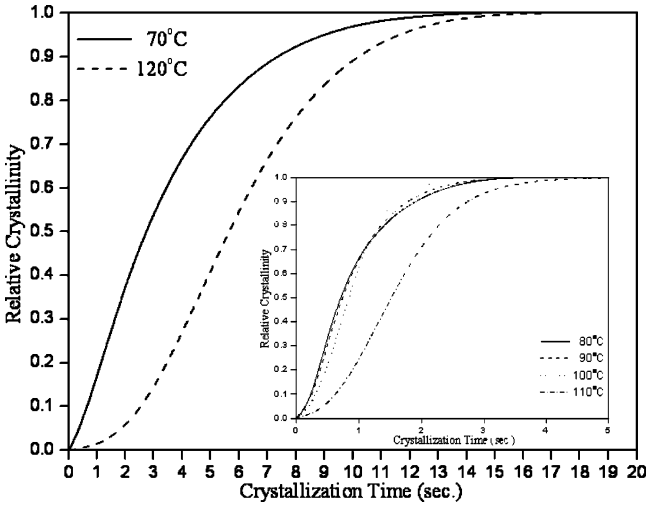

Figure 11. Plot of relative crystallinity versus crystallization time for oriented PS-PLLA samples isothermally crystallized at different temperatures from ordered melt at 160 °C.

perature, following the typical Hoffmann−Weeks prediction. In contrast, the melting temperature of the PS-PLLA block copolymer remains approximately constant when $T_{c,PLLA} < T_{g,PS}$. However, a dramatic change in melting is seen when crystallization takes place at temperatures above $T_{g,PS}$ (Figure 14); even the sample appears to have a crystallinity equivalent to that crystallized at lower temperatures (below $T_{g,PS}$). Because the value of long period shows no significant change from SAXS, we speculate that the PLLA crystallites become thicker due to the weaker effect of soft confinement than that of hard confinement during PLLA crystallization.

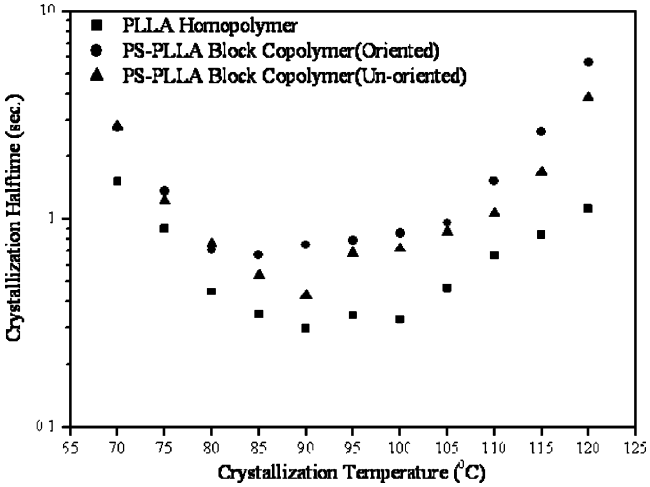

Figure 12. Plot of crystallization halftime ($t_{1/2}$) versus crystallization temperature for unoriented and oriented PS-PLLA samples as well as homopolymer PLLA isothermally crystallized at different temperatures from ordered melt at 160 °C.

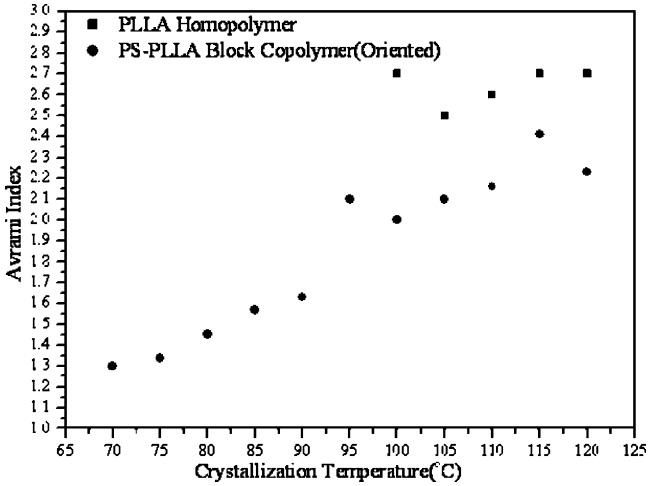

Figure 13. Plot of Avrami index (n) versus crystallization temperature (T_c) for homopolymer PLLA and oriented PS-PLLA samples isothermally crystallized at different temperatures from ordered melt at 160 °C.

Similar crystallization and melting behaviors were observed in both oriented and unoriented samples. The only discrepancy between them is the slight change of the crystallization kinetics due to the effect of grain boundary on microphase-separated domains. The crystallization process in unoriented samples exhibits a higher crystallization rate as compared to that in the oriented sample (Figure 12).

Possible Origins of the Undulation in Lamellar Morphology. The undulation phenomenon in the microphase-separated morphology has been observed before, where several mechanisms have been proposed to explain this behavior.[37−46] One of the most acceptable mechanisms attributes the undulation process to temperature fluctuation, particularly at temperatures near T_{ODT} or the ordered phase transition.[37−40] Yet this mechanism cannot be used to explain the observations in this study, as the chosen experimental temperatures are well below the T_{ODT} of PS-PLLA block copolymer. Another possible mechanism for the undulation process is the stress-induced structural changes, which is more reasonable. The stress-induced undulation has been

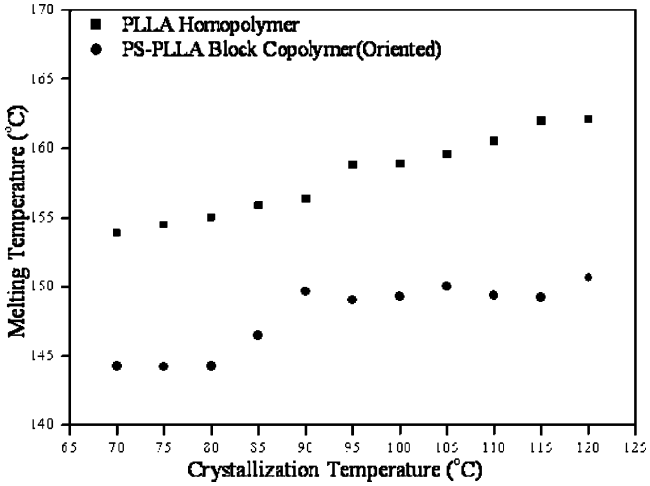

Figure 14. Plot of melting temperature (T_m) versus crystallization temperature (T_c) for homopolymer PLLA and oriented PS-PLLA samples isothermally crystallized at different temperatures from ordered melt at 160 °C.

theoretically predicted to occur in a lamellar diblock copolymer under extensional or shear fields.[41,42] This field-induced structural instability is similar to the relaxation of the distortion energy in smectic A liquid crystal systems,[46−48] where undulation occurs due to the extensional distortion of high strength mesogens under constraining boundary conditions. This allows a significant part of the deformation to be accommodated by undulation of the layered structures. Corresponding experimental observations have also been identified.[43,44] For block copolymers, the detailed mechanisms for the perpendicularly aligned stress-induced undulation, particularly for stretching-induced undulation, were thoroughly examined by Thomas and co-workers.[45] They suggested that the undulation instability is a highly cooperative phenomenon of a single-crystal-like arrangement of layers between confining external boundaries, where the phase boundary conditions force the adjacent layers to maintain a parallel orientation.

In this study, we report a similar behavior for the crystallization-induced undulation behavior even though no external stress was explicitly applied. It is conceivable that the undulation instability induced by crystallization can also be attributed to the stress field created during PLLA crystallization, which affects the stability of the final nanostructures in the separated phase. At a temperature above the glass transition of PS, the crystallization growth of PLLA chains can take different pathways to form the ordered structure. If the nucleation mode is heterogeneous (the crystallization temperature approaches $T_{g,PS}$), it is possible that the nucleation process is initiated from the interface. As the stress is built up at the interface with crystallization, the strong segregation strength of microphase separation that inhibits the breakout of microdomains would lead to the stress-relaxation process by relieving the constraint energy and adopting undulation instability. This would be a particularly easier process at higher temperatures (above $T_{g,PS}$) when the PS microdomain

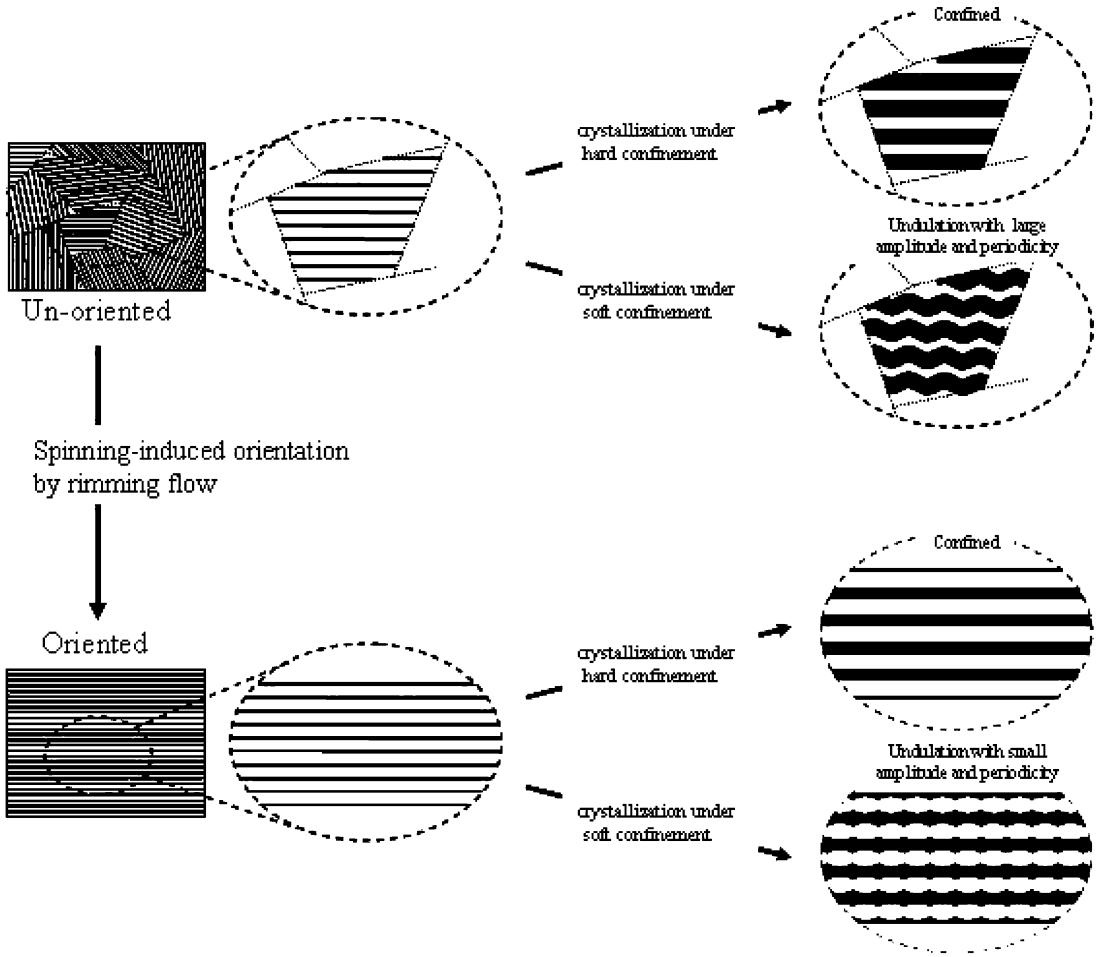

Figure 15. Illustration of the effects of crystallization on the PS-PLLA morphology from hard to soft confinement in unoriented and oriented samples.

becomes a rubbery phase. Thus, we argue that a critical strain is needed to form an undulated interface boundary, which would relax the stretching of the chain conformation and balance the enthalpic penalty due to undulation after stress relaxation. For a given strain above the critical value, larger amplitude is associated with a longer undulation periodicity, which is driven by a significant dilation of the layers near the external boundary. This behavior has been reported experimentally[45] and theoretically.[41] Thus, the sample distance between the imposed boundary conditions is important in determining the critical strain and the periodicity of the undulation instability.

The absence of the crystallization-induced undulation in the PS-PLLA lamellar phase at lower temperatures ($T_{c,PLLA} < T_{g,PS}$, i.e., hard confinement) can be attributed to one major reason. That is, during hard confinement crystallization, the stress-build up in the PLLA phase cannot overcome the modulus of the confining glassy PS layers, thus leaving the original morphology unchanged. It is also noted that the crystalline PLLA density gradually approaches the amorphous PLLA density as the temperature decreases to ca. 70 °C. This may also be one of the reasons that no undulation has been observed for PS-PLLA at low temperature. Nevertheless, it is just happened that the crystallization process at these temperatures also becomes dominated by the homogeneous nucleation. We do not believe the change from homogeneous nucleation to heterogeneous nucleation in the PLLA phase is directly responsible for the occurrence of the undulation behavior.

It is interesting to note that the oriented PS-PLLA sample exhibits a smaller undulation (in amplitude and in periodicity) than that in unoriented samples (Figure 15). These results can be explained as follows. It is possible that both grain boundaries and defects on the interfaces of microdomains can serve as nucleation sites during heterogeneous nucleation-dominated crystallization. If more grain boundaries exist, as in unoriented PLLA samples, then the crystallization-induced undulation behavior should be more enhanced, which is consistent with our observations. In addition, we found that the unoriented sample exhibited a faster crystallization rate (Figure 12), which is also consistent with the notion that heterogeneous nucleation may be induced by the grain boundary. In contrast, the oriented sample showed less overall grain boundary interfaces (or less heterogeneous nucleation sites), thus leading to a smaller undulation after crystallization.

Conclusion

Crystallization from hard confinement to soft confinement under strong segregation strength in crystallizable block copolymer, PS-PLLA (having $T_{g,PS} \approx 85$ °C, $T_{g,PLLA} \approx 45$ °C, $T_{m,PLLA} \approx 150$ °C, and predicted $T_{ODT} \approx 400$ °C), in microphase-separated lamellar morphology has been studied. The effects of crystallization on microphase-separated lamellae were found to exhibit a strong dependence on the confined environments. A confined morphology was observed during crystallization under hard confinement, whereas an undulated morphology was obtained under soft confinement. The crystallography, crystallization, and melting behavior under confinement of the PLLA block were studied. Based on thermal analysis and crystallization kinetics data, the PLLA blocks under confinement show a significant transition from homogeneous to heterogeneous nucleation once the crystallization temperature approached $T_{g,PS}$. A strong correlation between the crystallization kinetics and the morphological evolution was identified. The melting behavior was also found to be affected by the changes of the morphology. As evidenced by 2D SAXS and WAXS experiments, the PLLA crystalline chains were oriented perpendicular to the lamellae. Crystallization-induced undulation instability, similar to the stress-induced mechanism, was thus proposed to interpret the morphological changes.

Acknowledgment. R.-M.H. acknowledges the financial support of the National Science Council (NSC) of Taiwan (NSC-92-2216-E-007-031). R.M.H. would also like to thank Ms. P.-C. Chao of the Regional Instruments Center at NCHU for her help with the TEM experiments. The SAXS synchrotron beamline X27C was supported by the Department of Energy (Grant DE-FG02-99ER 45760).

References and Notes

(1) Bates, F. S.; Fredrickson, G. H. *Annu. Rev. Phys. Chem.* **1990**, *41*, 525.
(2) Whitesides, G. M.; Grzybowski, B. *Science* **2002**, *295*, 2418.
(3) Nojima, S.; Kato, K.; Yamamoto, S.; Ashida, T. *Macromolecules* **1992**, *25*, 2237.
(4) Ryan, A. J.; Hamley, I. W.; Bras, W.; Bates, F. S. *Macromolecules* **1995**, *28*, 3860.
(5) Yang, Y.-W.; Tanodekaew, S.; Mai, S.-M.; Booth, C.; Ryan, A. J.; Bras, W.; Viras, K. *Macromolecules* **1995**, *28*, 6029.
(6) Zhu, L.; Chen, Y.; Zhang, A.; Calhoun, B. H.; Chun, M.; Quirk, R. P.; Cheng, S. Z. D.; Hsiao, B. S.; Yeh, F.; Hashimoto, T. *Phy. Rev. B* **1999**, *60*, 10022.
(7) Cohen, R. E.; Cheng, P. L.; Douzinas, K.; Kofinas, P.; Berney, C. V. *Macromolecules* **1990**, *23*, 324.
(8) Douzinas, K. C.; Cohen, R. E. *Macromolecules* **1992**, *25*, 5030.
(9) Cohen, R. E.; Bellare, A.; Drzewinski, M. A. *Macromolecules* **1994**, *27*, 2321.
(10) Khandpur, A. K.; Macosko, C. W.; Bates, F. S. *J. Polym. Sci., Part B: Polym. Phys.* **1995**, *33*, 247.
(11) Liu, L.-Z.; Yeh, F.; Chu, B. *Macromolecules* **1996**, *29*, 5336.
(12) Hamley, I. W.; Fairclough, J. P. A.; Terrill, N. J.; Ryan, A. J.; Lipic, P. M.; Bates, F. S.; Towns-Andrews, E. *Macromolecules* **1996**, *29*, 8835.
(13) Hamley, I. W.; Fairclough, J. P. A.; Ryan, A. J.; Bates, F. S.; Towns-Andrews, E. *Polymer* **1996**, *37*, 4425.
(14) Quiram, D. J.; Register, R. A.; Marchand, G. R.; Adamson, D. H. *Macromolecules* **1998**, *31*, 4891.
(15) Hamley, I. W.; Fairclough, J. P. A.; Bates, F. S.; Ryan, A. J. *Polymer* **1998**, *39*, 1429.
(16) Weimann, P. A.; Hajduk, D. A.; Chu, C.; Chaffin, K. A.; Brodil, J. C.; Bates, F. S. *J. Polym. Sci., Part B: Polym. Phys.* **1999**, *37*, 2053.
(17) Zhu, L.; Cheng, S. Z. D.; Calhoun, B. H.; Ge, G.; Quirk, R. P.; Thomas, E. L.; Hsiao, B. S.; Yeh, F.; Lotz, B. *J. Am. Chem. Soc.* **2000**, *122*, 5957.
(18) Loo, Y. L.; Register, R. A.; Ryan, A. J. *Phys. Rev. Lett.* **2000**, *84*, 4120.
(19) Zhu, L.; Cheng, S. Z.-D.; Calhoun, B. H.; Ge, Q.; Quirk, R. P.; Thomas, E. L.; Hsiao, B. S.; Yeh, F.; Lotz, B. *Polymer* **2001**, *42*, 5829.
(20) Zhu, L.; Calhoun, B. H.; Ge, Q.; Quirk, R. P.; Cheng, S. Z.-D.; Thomas, E. L.; Hsiao, B. S.; Yeh, F.; Liu, L.; Lotz, B. *Macromolecules* **2001**, *34*, 1244.
(21) Ishikawa, S.; Ishizu, K.; Fukutomi, T. *Eur. Polym. J.* **1992**, *28*, 1219.
(22) Kofinas, P.; Cohen, R. E. *Macromolecules* **1994**, *27*, 3002.
(23) Quiram, D. J.; Register, R. A.; Marchand, G. R. *Macromolecules* **1997**, *30*, 4551.
(24) Mai, S.-M.; Fairclough, J. P. A.; Viras, K.; Gorry, P. A.; Hamley, I. W.; Ryan, A. J.; Booth, C. *Macromolecules* **1997**, *30*, 8392.
(25) Hillymer, M. A.; Bates, F. S. *Macromol. Symp.* **1997**, *117*, 121.
(26) Hamley, I. W.; Fairclough, J. P. A.; Bates, F. S.; Ryan, A. J. *Polymer* **1998**, *39*, 1429.
(27) Chen, H. L.; Hsiao, S. C.; Lin, T. L.; Yamauchi, K.; Hasegawa, H.; Hashimoto, T. *Macromolecules* **2001**, *34*, 671.

(28) Chen, H.-L.; Wu, J. C.; Lin, T.-L.; Lin, J. S. *Macromolecules* **2001**, *34*, 6936.
(29) Loo, Y.-L.; Register, R. A.; Ryan, A. J.; Dee, G. T. *Macromolecules* **2001**, *34*, 8968.
(30) Loo, Y.-L.; Register, R. A.; Ryan, A. J. *Macromolecules* **2002**, *35*, 2365.
(31) Lin, C. C.; Ko, B. T. *J. Am. Chem. Soc.* **2001**, *123*, 7973.
(32) Ho, R. M.; Chiang, Y. W.; Tsai, C. C.; Lin, C. C.; Ko, B. T.; Huang, B. H. *J. Am. Chem. Soc.* **2004**, *126*, 2704.
(33) Tsuji, H.; Ikada, Y. *Polymer* **1995**, *36*, 2709.
(34) Zalusky, A. S.; Olayo-Valles, R.; Wolf, J. H.; Hillmyer, M. A. *J. Am. Chem. Soc.* **2002**, *124*, 12761.
(35) Hoogsten, W.; Postema, A. R.; Pennings, A. J.; ten Brinke, G.; Zugenmaier, P. *Macromolecules* **1990**, *23*, 634.
(36) Cartier, L.; Okihara, T.; Ikada, Y.; Tsuji, H.; Puiggali, J.; Lotz, B. *Polymer* **2000**, *41*, 8909.
(37) Bates, F. S.; Koppi, K. A.; Tirrell, M.; Almdal, K.; Mortensen, K. *Macromolecules* **1994**, *27*, 5934.
(38) Krishnamoorti, R.; Modi, M. A.; Tse, M. F.; Wang, H. C. *Macromolecules* **2000**, *33*, 3810.
(39) Petr, S.; Nallet, F.; Almdal, K. *Macromolecules* **2001**, *34*, 1090.
(40) Petr, S.; Nallet, F.; Diat, O.; Almdal, K.; Panine, P. *Macromolecules* **2002**, *35*, 7287.
(41) Amundson, K.; Helfand, E. *Macromolecules* **1993**, *26*, 1324.
(42) Wang, Z.-G. *J. Chem. Phys.* **1994**, *100*, 2298.
(43) Drolet, F.; Chen, P.; Vinals, J. *Macromolecules* **1999**, *32*, 8603.
(44) Wang, H.; Newstein, M. C.; Krishnan, A.; Balsara, N. P.; Garetz, B. A. *Macromolecules* **1999**, *32*, 3695.
(45) Cohen, Y.; Albalak, R. J.; Dair, B. J.; Capel, M. S.; Thomas, E. L. *Macromolecules* **2000**, *33*, 6502.
(46) De Gennes, P. G.; Prost, J. *The Physics of Liquid Crystals*; Clarendon Press: Oxford, 1993.
(47) Clark, N. A.; Meyer, R. B. *Appl. Phys. Lett.* **1973**, *22*, 493.
(48) Delays, M.; Ribotta, R.; Durand, G. *Phys. Lett.* **1973**, *44A*, 139.

MA0492869